

Synthesis and Evaluation of Biphenyl Compounds as Kinesin Spindle Protein Inhibitors

by Jason P. Holland^{a)}, Albert Kang^{b)}, Susan Cohrs^{c)}, Svetlana V. Selivanova^{b)}, Selena Milicevic Sephton^{b)}, Thomas Betzel^{b)}, Daniel Frey^{d)}, Mara Wieser^{d)}, Rolf Jaussi^{d)}, Richard A. Kammerer^{d)}, Roger Schibli^{b)c)}, and Eliane Fischer^{*c)}

^{a)} Division of Nuclear Medicine and Molecular Imaging, Massachusetts General Hospital, and Department of Radiology, Harvard Medical School, 55 Fruit St., White 427, Boston, 02114, MA, USA (phone: +1-(617)-726-6107; fax: +1-(617)-726-6165; e-mail: holland.jason@mgh.harvard.edu)

^{b)} Institute of Pharmaceutical Sciences, Department of Chemistry and Applied Biosciences, ETH Zürich, CH-8093 Zürich

^{c)} Center for Radiopharmaceutical Sciences, Paul Scherrer Institute, CH-5232 Villigen PSI (phone: +41-56-310-2857; fax: +41-56-310-2849; e-mail: eliane.fischer@psi.ch)

^{d)} Laboratory of Biomolecular Research, Paul Scherrer Institut, CH-5232 Villigen PSI

Kinesin spindle protein (KSP), an ATP-dependent motor protein, plays an essential role in bipolar spindle formation during the mitotic phase (M phase) of the normal cell cycle. KSP has emerged as a novel target for antimetastatic anticancer drug development. In this work, we synthesized a range of new biphenyl compounds and investigated their properties *in vitro* as potential antimetastatic agents targeting KSP expression. Antiproliferation (MTT (= 3-(4,5-dimethylthiazol-2-yl)-2,5-diphenyl-2H-tetrazolium bromide)) assays, combined with fluorescence-assisted cell sorting (FACS) and *Western* blot studies analyzing cell-cycle arrest confirmed the mechanism and potency of these biphenyl compounds in a range of human cancer cell lines. Structural variants revealed that functionalization of biphenyl compounds with bulky aliphatic or aromatic groups led to a loss of activity. However, replacement of the urea group with a thiourea led to an increase in antiproliferative activity in selected cell lines. Further studies using confocal fluorescence microscopy confirmed that the most potent biphenyl derivative identified thus far, compound **7**, exerts its pharmacologic effect specifically in the M phase and induces monoaster formation. These studies confirm that chemical scope remains for improving the potency and treatment efficacy of antimetastatic KSP inhibition in this class of biphenyl compounds.

Introduction. – Hyperproliferation – the increased rate of cellular division – is a primary hallmark of cancer [1]. Many anticancer agents used in the clinic inhibit cell-cycle progression during either the synthesis (S) or mitotic (M) phase. Subsequent activation of checkpoints typically induces cell-cycle arrest or programmed cell death (apoptosis). Antiproliferative drugs can be subdivided into three main categories [2]: *i*) drugs that induce DNA damage and/or inhibit DNA repair mechanisms (*e.g.*, topoisomerase-II α inhibitors); *ii*) drugs that interfere with DNA synthesis in the S phase (*e.g.*, DNA intercalators (doxorubicin) and cross-linkers (cisplatin)); and *iii*) drugs that disrupt mitosis by inhibiting various components or functions of the mitotic spindle. This third class includes the taxanes (paclitaxel), epothilones, and *Vinca* alkaloids, each of which bind to microtubules (MTs) and disrupt the normal dynamic instability of the bipolar spindle through either stabilizing or destabilizing interactions. The efficacy of MT-targeted drugs resides in their ability to activate the M-phase

spindle checkpoint. Spindle checkpoint activation prevents the onset of anaphase and typically leads to cell death by mitotic catastrophe or mitotic slippage, followed by apoptosis during the subsequent growth phase (G_1 phase).

Although MT-targeted drugs have proven successful in the clinic [3], treatment often induces a range of unwanted side-effects including severe peripheral neuropathy and hematopoietic toxicity. These side-effects derive from the fact that MTs also play important roles in resting and differentiated cells like, for example, facilitating intracellular transport of proteins or vesicles. In efforts to circumvent the observed side-effects, new antimitotic agents directed toward crucial M-phase-specific kinase and kinesin motor proteins associated with bipolar spindle function have been the subject of intense investigations (*Fig. 1*) [2].

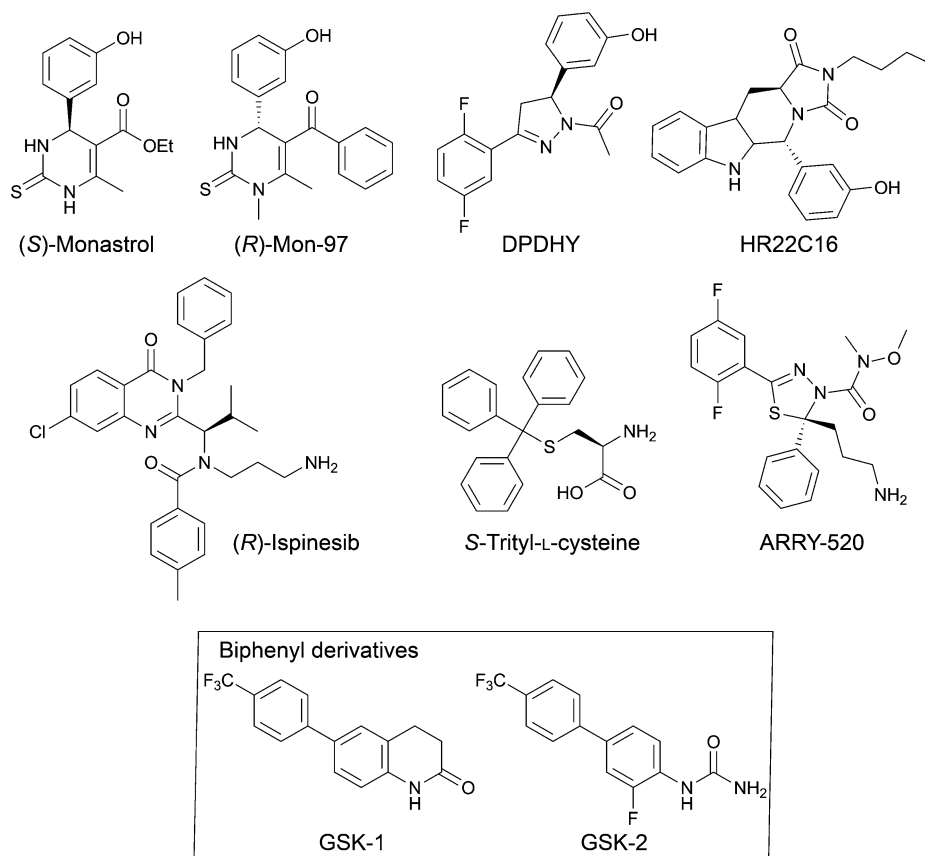


Fig. 1. Structures of selected allosteric KSP inhibitors

Recently, kinesin spindle protein (KSP, Kif11, hEg5, or kinesin-5) has emerged as a potential antimitotic target for drug discovery [4][5]. KSP is an ATP-dependent motor protein that binds MTs and is required at early stages in mitosis (during prophase and prometaphase) for both bipolar spindle formation and proper segregation of sister

chromatids [6]. Inhibition of KSP results in an unusual cell phenotype in which the two centrosomes fail to migrate to opposite poles of the cell, thereby leading to the formation of a characteristic monopolar (monoastral) spindle [4][7][8]. Systematic analysis of KSP mRNA expression levels revealed that, relative to neurons and fibroblasts, KSP is highly expressed in proliferating human tissue. Importantly, KSP protein levels were also shown to be overexpressed in various tumor tissues [8][9]. Preclinical studies have shown that kinesin inhibitors have fewer side-effects than MT-targeted agents, including reduced neuronal toxicity, and are also effective antiproliferation agents against paclitaxel-resistant tumors [10]. Further, several allosteric, ATP-noncompetitive KSP inhibitors such as ispinesib [11] and ARRY-520 [12] have been investigated in Phase-I/II clinical trials (*Fig. 1*).

In 2007, Luo *et al.* reported the first ATP-competitive, allosteric KSP inhibitors based on biphenyl derivatives [13]. Chemical optimization identified two lead compounds, GSK-1 and GSK-2, which were both characterized as ATP-competitive, but MT-noncompetitive KSP inhibitors with K_i values of 1.8 ± 0.2 and 8.8 ± 0.7 nM, respectively. Interestingly, the binding mode of these biphenyl compounds was found to be distinct from previous ATP-noncompetitive inhibitors such as the dihydropyrimidine (*S*)-monastrol and quinazolinone-derivative (*R*)-ispinesib. Further, GSK-1 and GSK-2 were shown to be potent antimetabolic agents with increased activity in ispinesib-resistant strains harboring the D130V mutant KSP; GSK-1 inhibits the proliferation of parental HCT-116 colorectal cancer cells (IC_{50} 36 nM) but showed increased potency (IC_{50} 0.5 nM) toward ispinesib-resistant HCT116-D130V cells [13].

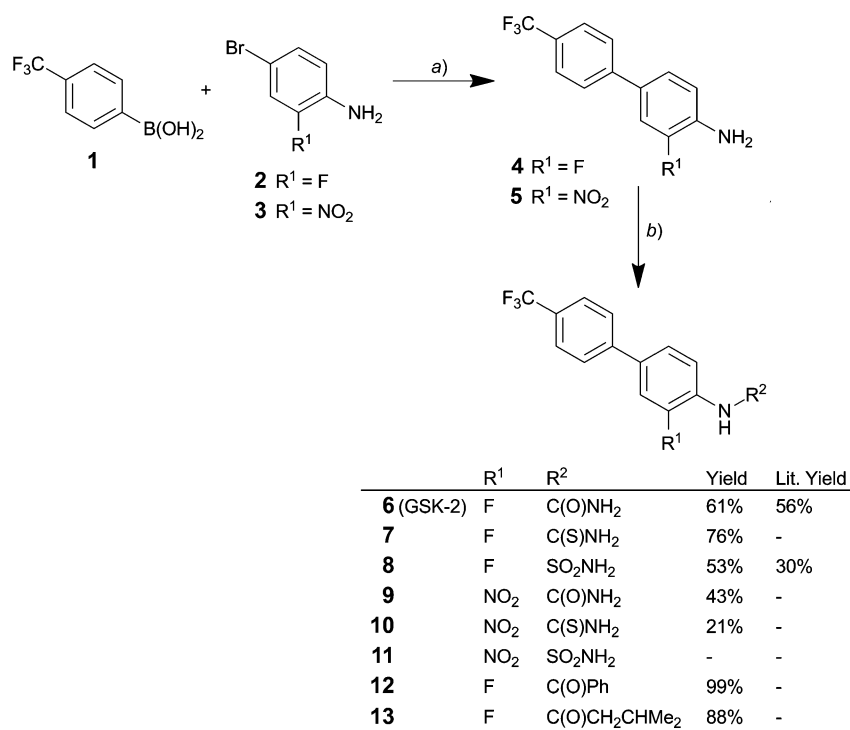
Following the discovery of biphenyl derivatives as novel KSP inhibitors, further studies probed the chemical scope of interaction with KSP by conducting structure–activity relationships (SARs) [14][15]. Parrish *et al.* synthesised 58 compounds with varying substituents on both phenyl rings [14]. They found that the *para*-trifluoromethyl (CF_3) substituent was a conserved feature of the pharmacophore required for KSP inhibition. This effect was also noted to be due to steric contributions related to the size rather than electronic properties of the CF_3 group. In addition, they found that the most potent analogs had a urea or sulfamide group in the *para*-position of the second phenyl ring.

Here, we present data evaluating several biphenyl compounds as potential KSP inhibitors. Specifically, we report the synthesis of a new, more active thiourea derivative and also the effect of functionalizing the urea group with aliphatic or aromatic moieties. The new compounds were studied by using a range of techniques including chemical characterization and protein inhibition assays *in vitro*. The effect of our compounds on various human cancer cells (prostate cancer cells: PC-3 and DU-145; ovarian cancer cells: SKOV-3; and breast cancer cells: MCF-7) was evaluated by using cellular growth inhibition assays (MTT (= 3-(4,5-dimethylthiazol-2-yl)-2,5-disphenyl-2*H*-tetrazolium bromide)), cell-cycle analysis with fluorescence-assisted cell sorting (FACS), and *Western* blot studies, as well as confocal fluorescence microscopy studies. From the outset, our hypothesis was that chemical modification of the terminal substituent on the biphenyl system could be made so as to facilitate the introduction of an [^{18}F]- or [^{11}C]-radiolabel for developing a novel positron-emitting radiotracer for noninvasive positron-emission tomography (PET) imaging of the drug pharmacokinetics and KSP expression *in vivo*. The aim of this work was to identify a lead biphenyl compound

that retained high biological activity and specificity toward KSP inhibition which could potentially be developed as radiolabelled analog.

Results and Discussion. – *Synthesis of Biphenyl Derivatives.* The synthesis of biphenyl derivatives **6–13** was accomplished in two-steps by using procedures modified from previous reports (*Scheme*) [14–16]. Where appropriate, the chemical identity and purity of all compounds has been fully characterized by using a range of techniques including thin-layer chromatography (TLC), melting points, ^1H -, ^{13}C -, and ^{19}F -NMR spectroscopy, high-resolution mass spectrometry, IR spectroscopy, and high-performance liquid chromatography (HPLC; *cf.* the *Exper. Part*). In the first step, the C–C bond linking the two aromatic groups in compounds **4** and **5** was formed by reaction of either compound **1** or **2** with compound **3** in a classical Pd-catalyzed ($[\text{Pd}(\text{PPh}_3)_4]$) *Suzuki* cross-coupling [17]. Compound **4** was isolated as a deep-red amorphous powder in 87% yield, whereas compound **5** was obtained as a white amorphous powder (77%). For synthesis of compounds **6–13**, the second step involved functionalization of the anilinic NH_2 group by reaction with chlorosulfonyl isocyanate (ClSO_2NCO), ammo-

Scheme. *Chemical Synthesis of Biphenyl Derivatives 6-13.*



a) Standard *Suzuki* coupling reactions with $[\text{Pd}(\text{PPh}_3)_4]$, K_2CO_3 (aq.), DMF, 100° , 24 h. *b)* For compounds **6** and **8**: ClSO_2NCO , r.t., 3 h; for **7** and **10**: ammonium thiocyanate (NH_4SCN), 140° , 15 h; for **9** and **11**: ClSO_2NCO , 70° , 5 h; for **12**: PhCOCl , 50° , 18 h; for **13**: 3-methylbutanoyl chloride, r.t., 24 h. Lit. = Yields reported in [14].

nium thiocyanate (NH_4SCN), benzoyl chloride (PhCOCl), or 3-methylbutanoyl chloride. In general, for compounds where $\text{R}^1 = \text{F}$, reaction yields were moderate to high (53–99%). However, due to solubility issues and difficulties associated with purification, yields for the NO_2 derivatives **9** and **10** were lower (21–43%), and it was not possible to isolate compound **11** using our standard chromatography methods. Nucleophilic aromatic substitution ($\text{S}_{\text{N}}\text{Ar}$) of the NO_2 group as R^1 by ^{18}F represents a potential (if in this case challenging) route to producing an ^{18}F -radiolabelled compound. Unfortunately, lack of access to the radiolabelling precursor hindered our efforts, and this route was not pursued further.

Density-Functional Theory (DFT) Calculations. Interestingly, unlike the ATP-noncompetitive KSP inhibitors (*Fig. 1*) for which extensive characterization of the binding mode and mechanism for KSP inhibition have been provided by the use of biochemical assays and crystallography [9], no crystal structure exists of a biphenyl compound bound to KSP. This is likely because biphenyl compounds are only active against MT-bound KSP. The heterogeneous chemical nature of MT samples makes co-crystallization difficult. In their SAR studies, *Parrish et al.* noted that linker atoms inserted between the two phenyl groups were not tolerated, and they proposed that, for an active conformation, the biphenyl group must remain close to planar [14]. To investigate this possibility further, we conducted DFT calculations to probe the electronic structure and preferred geometry of the biphenyl compounds (*Fig. 2*).

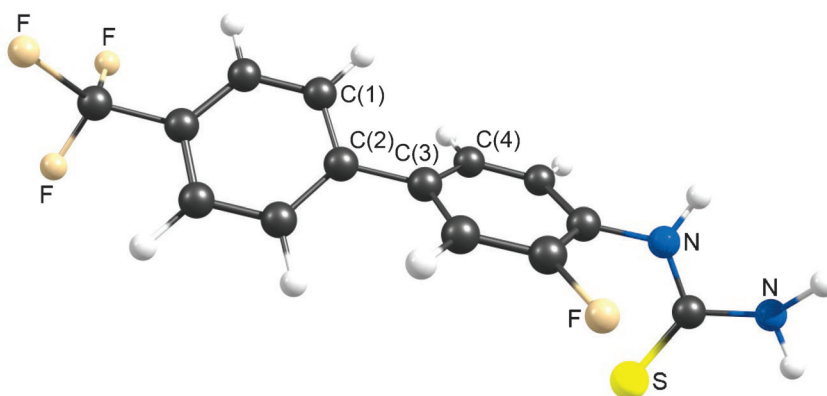


Fig. 2. DFT-Optimized geometry of compound **7** showing the twisted orientation between the two planes formed by the phenyl groups. Dihedral angle $\phi(\text{C}(1)\text{--C}(2)\text{--C}(3)\text{--C}(4)) = -39.0^\circ$.

The geometry of compound **7** was optimized by using Gaussian09 with the restricted B3LYP exchange-correlation functionals and the double- ζ 6-31++G(d,p) all electron basis set [18]. Contrary to the supposition by *Parrish et al.*, we found that, in the absence of a protein interaction, the biphenyl derivatives prefer a twisted orientation with a dihedral angle ϕ of -39.0° formed between the intersecting planes of the two aromatic rings. All other bond lengths and angles were found to be within normal parameters for small organic molecules [19]. In the absence of crystallographic data, the precise binding mode to KSP remains uncertain. However, we note that, although our DFT calculations predict a twisted geometry, a planar orientation cannot

be precluded, since stabilizing interactions between the biphenyl ligand and KSP may overcome the associated rotational energy barrier.

Kinesin Motor Protein Inhibition Assays. After successful isolation of the biphenyl compounds, we first investigated their ability to inhibit the enzymatic ATP-hydrolysis activity of KSP, as well as their selectivity for KSP vs. a panel of selected kinesin motor proteins (Fig. 3 and Table 1). Kinesins investigated included centromeric protein-E (CENP-E), mitotic centromere-associated kinesin (MCAK), kinesin heavy chain (KHC), and kinesin protein KIFC3. In addition, (*S*)-monastrol and (*R*)-ispinesib were used as positive controls, and the inactive stereoisomer (*S*)-ispinesib was used as a negative control for KSP inhibition.

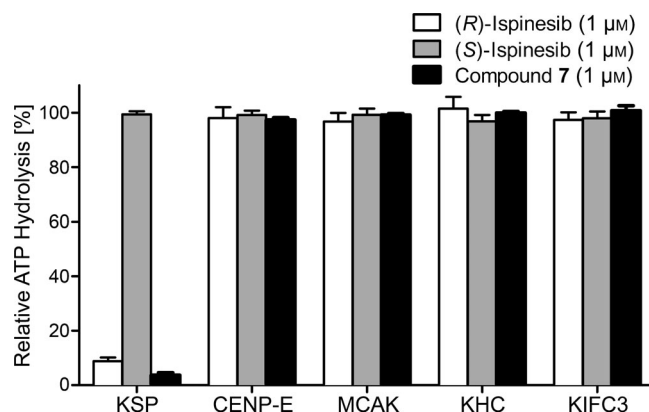


Fig. 3. Bar chart showing the specificity of compound **7** toward inhibition of KSP ATP hydrolysis *in vitro*. (*S*)-Monastrol and (*R*)-ispinesib were used as positive controls, while the inactive enantiomer, (*S*)-ispinesib, was used as a negative control.

Table 1. Kinesin Motor Protein ATP-Hydrolysis Activity [%] Relative to Untreated Controls

Compound (conc. [μM])	KSP	CENP-E	MCAK	KHC	KIFC3
(<i>S</i>)-Monastrol (10)	10.8 \pm 1.4	97.7 \pm 2.2	97 \pm 2.1	98.5 \pm 1.0	98.3 \pm 2.6
(<i>R</i>)-Ispinesib (1)	8.8 \pm 1.4	98 \pm 3.7	96.7 \pm 3.2	101.5 \pm 4.3	97.3 \pm 2.8
(<i>S</i>)-Ispinesib (1)	99.4 \pm 1.1	99.1 \pm 1.6	99.2 \pm 2.3	96.8 \pm 2.3	97.9 \pm 2.5
6 (1)	4.4 \pm 1.4	98.3 \pm 2.0	98.3 \pm 2.6	99.1 \pm 1.1	96.4 \pm 2.8
7 (1)	3.7 \pm 1.7	97.3 \pm 1.7	99.1 \pm 1.2	99.9 \pm 1.1	100.7 \pm 3.7
8 (1)	5.5 \pm 2.0	98.8 \pm 2.7	98.4 \pm 2.2	98.4 \pm 2.2	101.3 \pm 3.0
9 (1)	95.1 \pm 3.2	95.1 \pm 4.0	96.0 \pm 4.1	99.1 \pm 1.7	98.9 \pm 1.8
10 (1)	94 \pm 4.0	98.2 \pm 2.1	99.6 \pm 2.2	98.7 \pm 2.0	98.4 \pm 1.9
12 (100)	97.7 \pm 1.0	98.7 \pm 2.2	98.1 \pm 1.8	99.2 \pm 1.4	98.6 \pm 1.3
13 (100)	98.4 \pm 3.1	98.9 \pm 1.4	99.4 \pm 3.0	99.1 \pm 1.5	100.4 \pm 1.3

These assays indicated that only compounds **6–8** displayed activity and high selectivity towards KSP inhibition *in vitro*. These data demonstrate that NO₂ derivatives, *i.e.*, compounds **9** and **10**, as well as the terminally substituted compounds **12** and **13** failed to inhibit ATP-hydrolase activity of KSP or other kinesins studied. Unfortunately, these data also suggest that addition of a bulky aliphatic or aromatic (as typically required when using radiolabelled prosthetic groups for derivatizing small

molecules or peptides) is a not feasible route toward developing [^{18}F]- or [^{11}C]-radiolabelled compounds for this class of molecules.

Cellular-Growth-Inhibition Assays. We next investigated the potency of compounds **6–8** toward cellular-growth inhibition in a range of human cancer cell lines. Previous work on KSP inhibition has been focused on the use of drugs like ispinesib to inhibit the growth of colorectal carcinomas (using HCT116 cells) and ovarian cancer (SKOV-3 cells) [8]. In this work, we were interested in evaluating the potential of biphenyl compounds to inhibit KSP in different cell lines, namely prostate cancer lines PC-3 and DU-145, and the breast cancer cell line MCF-7. SKOV-3 Cells and treatment with (*S*)-monastrol were used as positive controls. Inhibition of cellular proliferation was determined by using the standard MTT assay, and data on the drug concentration at which proliferation was inhibited by 50% (growth-inhibition (GI_{50}) values) are compiled in Table 2. An example of the growth-inhibition curves generated for compounds **6–8** in DU-145 cells is shown in Fig. 4.

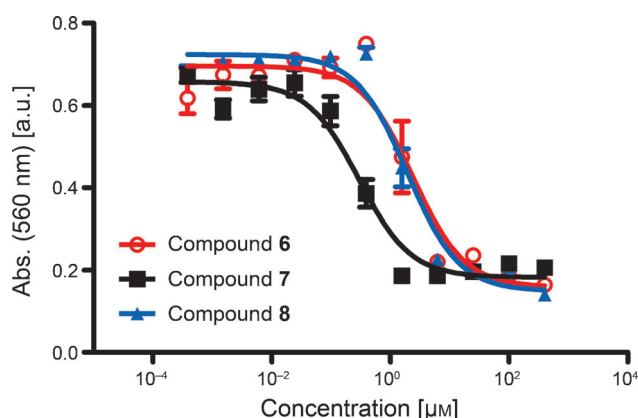


Fig. 4. Growth-inhibition curves derived from MTT assays of compounds **6–8** in DU-145 cells

Table 2. The GI_{50} Values [μM] for Various Biphenyl Derivatives Tested in Four Human Cancer Cell Lines

Compound	DU-145	PC-3	MCF-7	SKOV-3
(<i>S</i>)-Monastrol	159 ± 57	57.0 ± 17.8	42.7 ± 21.3	11.4 ± 2.6
6	1.19 ± 0.52	1.76 ± 0.54	0.46 ± 0.15	1.59 ± 0.54
7	0.15 ± 0.05	0.62 ± 0.24	0.37 ± 0.16	0.52 ± 0.16
8	0.97 ± 0.29	39.3 ± 23.8	0.38 ± 0.17	0.45 ± 0.16
9	NM ^{a)}	458 ± 474	NM	NM
10	NM	418 ± 410	NM	NM

^{a)} NM=Not measured.

The MTT data indicate that after 44 h incubation, biphenyl compounds **6–8** were found to be active toward all four cell lines. In particular, the novel thiourea compound **7** was found to inhibit DU-145 cellular proliferation with a GI_{50} value of $0.15 \pm 0.05 \mu\text{M}$. In comparison, the published urea analog (**6**; GSK-2) was found to be eight fold less potent (GI_{50} $1.19 \pm 0.52 \mu\text{M}$) in the same cells. Interestingly, this result was not

reproduced across all cell lines. In general, PC-3 and SKOV-3 cells were found to be less sensitive toward treatment with biphenyl drugs than DU-145 and MCF-7 cells. In addition, we also tested NO₂ derivatives **9** and **10** in PC-3 cells; both compounds were found to be inactive at μM concentrations, thus confirming our results from the protein inhibition assays (*vide supra*). First, these antiproliferative data indicate that minor structural or electronic changes in the biphenyl compound, such as replacing O with S (urea to thiourea) can induce comparatively large effects in their ability to inhibit cellular growth. Second, our data also point toward a pronounced cell-line dependence in the efficacy of KSP inhibition using biphenyl-based drugs. Reasons for this cell-line dependence remain unclear.

Cell-Cycle Analysis. To confirm that the antiproliferative effects observed in the MTT assays were the result of inhibition of cellular proliferation in the M phase, we investigated changes in cell-cycle population numbers upon treatment with the biphenyl drugs. Cells were treated with 1.0 μM concentrations of compounds **6–8** for a period of 24 h before staining with propidium iodide, and using fluorescence-assisted cell sorting (FACS) to analyse the number of cells in various stages of the cell cycle (G₁, S, and G₂/M phases). FACS Data for treatment of cells with the most potent compound **7** are presented in Table 3.

Table 3. Percentage of Cells in the G₁, S, and G₂/M Phases of the Cell Cycle upon Treatment with Either Vehicle (<1% DMSO in medium) or Compound **7** (1.0 μM) at 37 °C for 24 h

Cell phase	Cell line							
	DU-145		PC-3		MCF-7		SKOV-3	
	Control	Treated	Control	Treated	Control	Treated	Control	Treated
G ₁	57.8	35.9	39.6	13.9	54.9	23.4	56.9	5.8
S	6.5	11.6	12.1	14.9	20.0	11.9	19.7	14.8
G ₂ /M	31.6	47.9	39.8	62.6	21.7	60.8	20.0	69.5

In each cell line, treatment with compound **7** led to a dramatic shift in the number of cells found within the G₂/M phase of the cell cycle compared to vehicle-treated (<1% DMSO in medium) controls. For example, in SKOV-3 cells, treatment with **7** induced an increase in the G₂/M-phase population from 20 to *ca.* 70% of cells. Somewhat surprising was the small shift observed for the more sensitive DU-145 cells (G₂/M-phase control, 32%; treated, 48%). For DU-145 cells, we noted that a greater number of the cells were found to be apoptotic, and hence, excluded from the cell-cycle analysis by FACS gating. This observation is consistent with the MTT assays which revealed that DU-145 cells are particularly sensitive toward KSP inhibition. After only 24 h incubation, FACS data indicated that these drugs induce M-phase arrest in all cell lines, but, at this point, the cellular response diverges: DU-145 cells undergo rapid apoptosis (likely in the M phase due to mitotic catastrophe), whereas less sensitive lines such as PC-3 and SKOV-3 cells appear to remain in G₂/M-phase arrest or undergo mitotic slippage, followed by apoptosis in the G₁ phase. These data are consistent with the known mechanism of action of KSP inhibition with other inhibitors, including monastrol, ispinesib, and progenitor biphenyl compounds [4][8][13].

Western-Blot Protein Analysis. As confirmation of the induced M-phase arrest, we measured relative changes in the concentration of three protein markers displaying characteristic expression levels in different stages of the cell cycle by using *Western blotting* (Fig. 5). Here, we interrogated the change in expression levels of cyclin B1, cyclin E, and phospho-histone H3 (PHH3) as markers of the G₂/M and G₁/S phases and of mitosis, respectively. In all experiments, glyceraldehyde 3-phosphate dehydrogenase (GAPDH) was used as a protein loading control. The *Western blot* data provide further demonstration of the G₂/M-phase cell-cycle arrest induced up on treatment with compound **7**. With the exception of PHH3 levels in DU-145, markedly increased levels of both cyclin B1 and PH3 were observed across all cell lines after treatment. Furthermore, although control DU-145 and PC-3 cells showed only low levels of cyclin E, treatment did induce a loss of this protein marker, consistent with cell-cycle arrest in the G₂/M phase and the hypothesis that cell lines which are particularly sensitive to

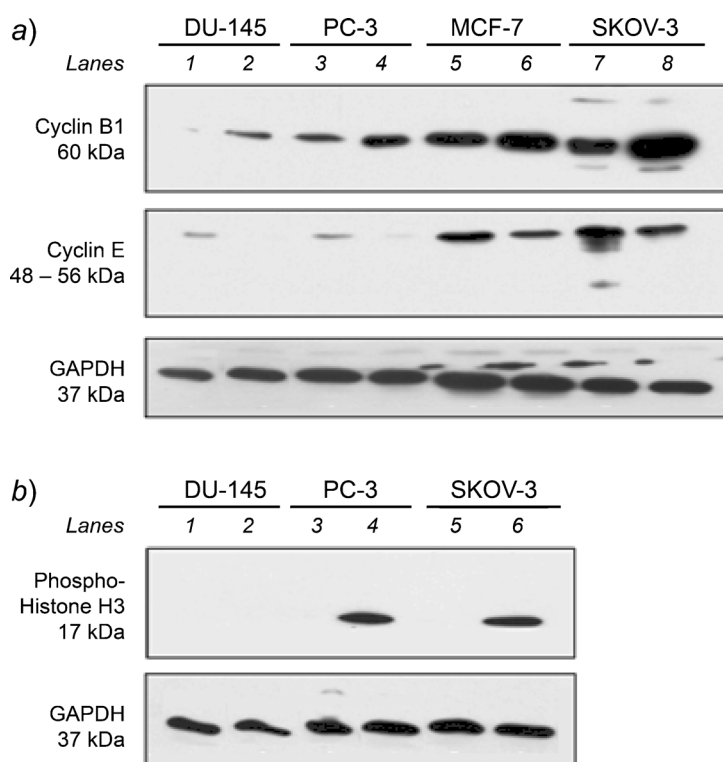


Fig. 5. Western-blot data showing the relative change in cell-cycle protein marker expression between cells treated with compound **7** and control cells. *a*) Relative expression levels of cyclin B1 and cyclin E as markers of the G₂/M phase and G₁/S phase, respectively. Numbers indicate Lanes 1–8: DU-145 (Lanes 1 and 2); PC-3 (Lanes 3 and 4); MCF-7 (Lanes 5 and 6); SKOV-3 (Lanes 7 and 8). *b*) Relative expression of phospho-histone 3 (PH3) as a mitosis marker lanes. DU-145 (Lanes 1 and 2); PC-3 (Lanes 3 and 4); SKOV-3 (Lanes 5 and 6). In both gels, glyceraldehyde 3-phosphate dehydrogenase (GAPDH) was used as a protein loading control.

KSP inhibition (like DU-145) undergo apoptosis resulting from mitotic catastrophe, as opposed to mitotic slippage and G₁-phase apoptosis.

Confocal Fluorescence Microscopy Studies. After having established the relative sensitivity of various human cancer cell lines toward treatment with biphenyl drugs and elucidated the likely mechanism of action, we next investigated the induced phenotypic effects using confocal fluorescence microscopy. The primary roles of KSP are associated with bipolar spindle formation and force generation on interpole MTs. Inhibition of KSP is known to induce M-phase arrest during prophase/prometaphase, which prevents separation of the two centrosome to opposite poles of the cell. Thus, KSP inhibition leads to a failure to establish a functional bipolar spindle, and gives rise to a characteristic monoaster phenotype [4].

Human cancer cells were grown for 22 h on 8-well-chambered microscope slides, before treating with either compound **7** (1.0 μM) or vehicle (< 1% DMSO in medium) at 37 °C for 24 h. Cells were then fixed and permeabilized before staining with an anti- α -tubulin antibody (and a secondary antibody labelled with *Alexa 568*), to probe the structure of the MT network, and *Hoechst 33342* to stain for DNA. Selected confocal fluorescence microscopy images are presented in *Fig. 6*.

In the control (vehicle-treated) SKOV-3 cells, we observed cells undergoing normal mitotic division in which a well-defined bipolar spindle, with the chromosomes aligned on the metaphasic plate, was clearly visible (*Fig. 6, d*). In contrast, upon examination of cells treated with compound **7**, we observed that the majority of cells in the samples treated with compound **7** exhibited a monoaster phenotype (*Fig. 6, a–c*). Results were confirmed by using (*R*)-ispinesib and (*S*)-ispinesib as positive and negative controls, respectively (data not shown).

Interestingly, we also observed that not all of the cells in the treated samples displayed a monoaster spindle (*Fig. 6, b*). Due to the restricted expression of KSP in the early stages of mitosis, treatment with KSP inhibitors such as compound **7** induces M-phase arrest in mitotic cells but fails to affect cells in interphase. Thus, cells which did not enter M phase during the treatment window were not affected by the drugs. These data are congruent with the results obtained from FACS and *Western* blot analysis where we observed an increase in the accumulation of cells in the G₂/M phase. Taken together, our experimental data provide compelling evidence that the antiproliferative effect of biphenyl derivatives **6–8** in a range of human cancer cell lines resides in their inhibition of KSP.

Conclusions. – Here, we reported the synthesis and *in vitro* characterization of a range of biphenyl compounds as inhibitors of KSP and potential antimetabolic agents. Replacement of the urea functionality with a thiourea led to an increased potency of the compounds toward growth inhibition in a range of human cancer cell lines. Structural modification centered on functionalizing the terminal amine group with a bulky aliphatic or aromatic group was found to be detrimental to KSP inhibition activity. The nature of the antiproliferative effects observed for compounds **6–8** was evaluated further by using a range of assays *in vitro*, including kinesin motor protein inhibition assays, FACS, *Western* blot analysis, and confocal fluorescence microscopy. These data confirmed that compound **7**, to the best of our knowledge, the most potent antiproliferative biphenyl derivative identified thus far, exerts its pharmacologic effect

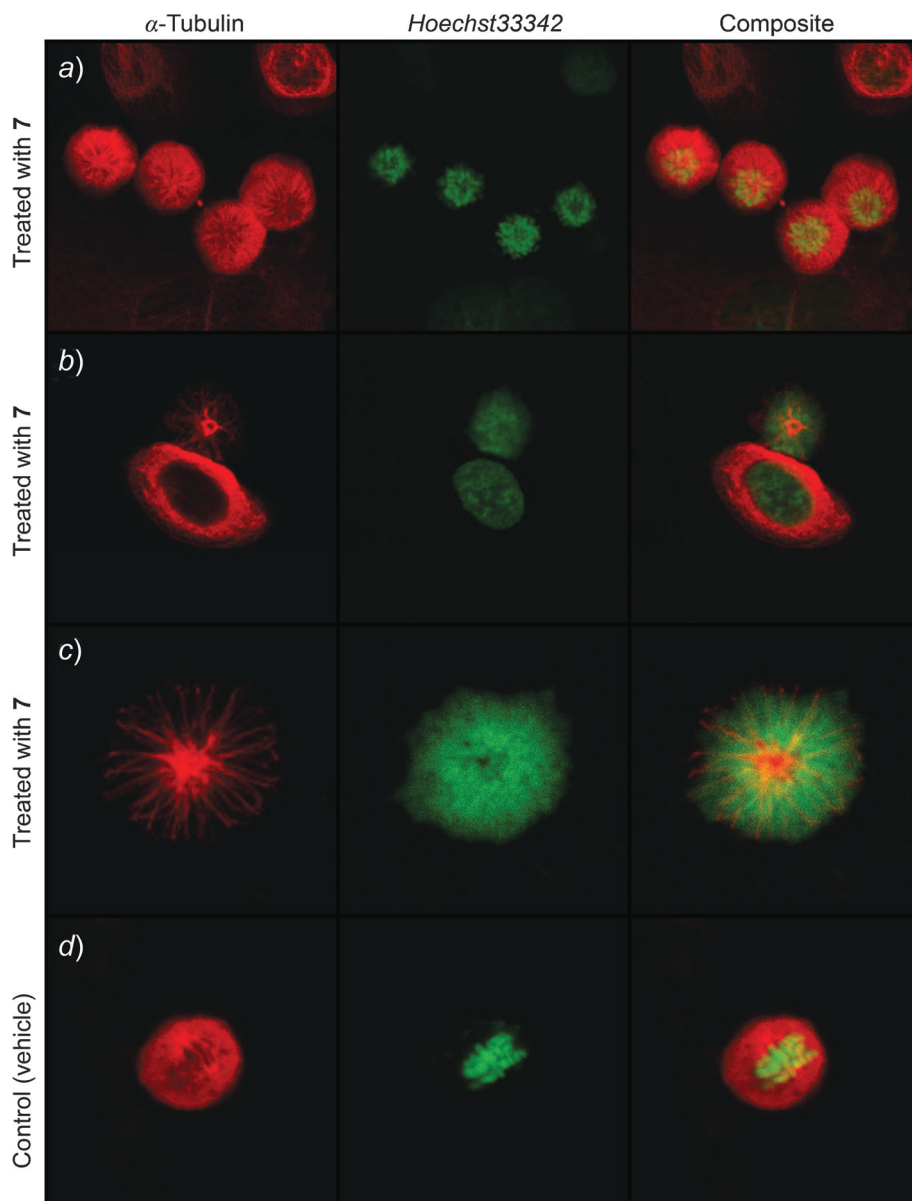


Fig. 6. Representative confocal fluorescence-microscopy images showing the effects of treatment of SKOV-3 cells with compound **7** at $1.0 \mu\text{M}$ after incubation at 37° for 22 h. a) A collection of four cells displaying the characteristic monoaster phenotype indicative of KSP inhibition and M-phase arrest. b) Two SKOV-3 cells in the same sample. The cell above displays a monoaster spindle whereas the control cell (below) remains in the growth phase. c) Magnified view of the monoaster formation showing MTs radiating from the center of the cell and a diffuse pattern of DNA staining. d) A representative image of a vehicle-treated SKOV-3 cell undergoing normal mitosis (anaphase). For full microscopy details, including magnification powers, see the *Exper. Part*.

via inhibition of KSP and induced M-phase arrest. Unfortunately, our structure–activity-relationship data indicate that appending the biphenyl compounds with bulky aliphatic or aromatic substituents is not a viable route for radiolabelling this class of molecules. Due to the complications of synthesizing the NO₂ derivatives and the likely low yields from attempts at direct [¹⁸F]-radiolabelling by an S_NAr mechanism, we conclude that these two approaches are not suitable for radiolabelling these biphenyl compounds. Alternative approaches involving [¹⁸F]-radiolabelling of the CF₃ group are under development.

Funded in part by the *ETH Fellowship Program* (FEL-01-10-1; JPH). We thank Dr. *Aristeidis Chiotellis* and *Cindy Fischer* for helpful discussions and advice regarding chemical synthesis and chromatography. We also thank Drs. *Tobias Schwarz* and *Joaquim Hehl* at the Light Microscopy Centre, ETH Zurich, for technical support regarding fluorescence microscopy studies.

Experimental Part

General. Standard laboratory techniques were employed when handling H₂O-sensitive reagents. All solvents and reagents were used as received from the supplier unless otherwise noted. Flash column chromatography (FC) was performed by using silica gel (*BDH*) according to the method of *Still et al.* [20]. TLC was performed on aluminium plates pre-coated with silica gel (0.2 mm, *Merck 60 F₂₅₄*), visualized by using UV fluorescence (254 and 366 nm) and KMnO₄ staining. RP-HPLC was performed on a *Merck Hiachi* HPLC (monitoring at a wavelength of 254 nm) equipped with a *LUNA 5μ C18* column (5 μm, 250 × 4.60 mm), eluting with an isocratic mobile phase of 60% MeCN and H₂O with 0.1% CF₃COOH (TFA) at a flow rate of 1.0 ml/min unless otherwise specified. M.p.: *Büchi 535* melting-point apparatus. IR Spectroscopy: *Jasco FT/IR-6200*, *OMNILAB* spectrometer. ¹H-, ¹³C-, and ¹⁹F-NMR spectra: at 400, 100, and 376 MHz, resp., on a *Bruker Ultra-Shield AV400* spectrometer; chemical shifts (δ(H), δ(C), and δ(F)) are expressed in ppm, referenced to the residual solvent resonance of (D₆)DMSO or CDCl₃ for ¹H- and ¹³C-NMR, and to the internal standard resonance of CFCl₃ for ¹⁹F-NMR, coupling constants (*J*) to the nearest 0.1 Hz. ESI-MS (*m/z* (rel. %)) and HR-ESI-MS: *Bruker Daltonics maxis* (UHR-TOF) *Compass 1.3* spectrometer.

Syntheses. *3-Fluoro-4-(trifluoromethyl)[1,1'-biphenyl]-4-amine* (**4**). To *4-bromo-2-fluoroaniline* (**2**; 1.20 g, 6.32 mmol, 1.2 equiv.) and *[4-(trifluoromethyl)phenyl]boronic acid* (**1**; 1.00 g, 5.27 mmol, 1.0 equiv.) were added 2.0M aq. K₂CO₃ (8.78 ml, 55.3 g K₂CO₃ in 200 ml H₂O) and DMF (8.78 ml) at r.t., and the mixture was stirred for 15 min at this temp. to give a pale yellow soln. [Pd(PPh₃)₄] (304 mg, 263 mmol, 0.05 equiv.) was then added, and the mixture was heated at 125° for 24 h under N₂. The mixture was subsequently cooled to r.t., poured onto 50% aq. NaHCO₃, then extracted with Et₂O (3 × 70 ml), dried (Na₂SO₄), filtered on a pad of silica gel with *Celite*, and concentrated under reduced pressure. Purification by FC (0–15% AcOEt/hexane) gave **4** (1.11 g, 87%). White amorphous powder. *R_f* (30% AcOEt/hexane) 0.57. M.p. 93–94°. ¹H-NMR ((D₆)DMSO): 7.80 (*d*, *J* = 8.2, F₃CC(CH)₂); 7.71 (*d*, *J* = 8.3, F₃C(CH)₂(CH)₂CC); 7.45 (*dd*, *J* = 2.1, 13.1, FCCH); 7.33 (*dd*, *J* = 2.0, 8.3, H₂NCCHCHCC); 6.86 (*q*, *J* = 8.4, 9.4, H₂NCCH); 5.45 (*br. s*, NH₂). ¹³C-NMR ((D₆)DMSO): 151.9 (CNH₂); 149.6 (CF); 143.4 (CCCHCF); 137.1 (CCF₃); 137.0 (FCCHCC); 126.0 (F₃CC(CH)₄C); 125.6 (CF₃); 123.1 (2 C, CCCHCH); 116.35 (*d*, *J* = 10.0, H₂NCCH); 113.3 (*d*, *J* = 20, FCCH). ¹⁹F-NMR ((D₆)DMSO): –60.7 (*s*, CF₃); –134.7 (*dd*, *J* = 9.5, 13.3, arom. F). ESI-MS: 255 (100, [M+H]⁺). HR-ESI-MS: 256.2227 ([M+H]⁺, C₁₃H₁₀F₄N⁺; calc. 256.0744). Data are in accordance with those in [14].

3-Nitro-4-(trifluoromethyl)[1,1'-biphenyl]-4-amine (**5**). To *4-bromo-2-nitroaniline* (**3**; 500 mg, 2.30 mmol, 1.0 equiv.) and **1** (525 mg, 2.76 mmol, 1.2 equiv.) were added 2.0M aq. K₂CO₃ (3.78 ml) and DMF (3.78 ml) at r.t., and the mixture was stirred for 15 min. [Pd(PPh₃)₄] (128 mg, 0.111 mmol, 0.05 equiv.) was then added, and the mixture was heated at reflux under N₂ and stirred at 100° for 21 h. The mixture was subsequently cooled, poured onto 50% aq. NaHCO₃, extracted with Et₂O (3 × 70 ml), dried (Na₂SO₄), filtered on a pad of silica gel with *Celite*, and concentrated under reduced pressure. Purification by FC (10–50% AcOEt/hexane) gave compound **5** (501 mg, 77%). Deep-red amorphous

powder. R_f (70% AcOEt/hexane) 0.30. M.p. 154–155°. $^1\text{H-NMR}$ ((D_6) DMSO): 7.68 (*s*, $\text{F}_3\text{CC}(\text{CH})_2(\text{CH})_2$); 6.93 (*d*, $J = 2.1$, O_2NCCH); 6.82 (*dd*, $J = 2.1$, 8.0, $\text{H}_2\text{NCCHCHCC}$); 6.60 (*d*, $J = 8.0$, H_2NCCH); 4.69 (*s*, NH_2). $^{13}\text{C-NMR}$ ((D_6) DMSO): 145.2 (CNH₂); 136.1 (O_2NCCHC); 135.2 (O_2NCCHCC); 128.7 (CCF₃); 127.0 (CNO₂); 125.7 ($\text{F}_3\text{CC}(\text{CH})_4\text{C}$); 125.5 (CF₃); 116.2, (CCCHCH); 114.5 (H_2NCCH); 112.5 (O_2NCCH). $^{19}\text{F-NMR}$ ((D_6) DMSO): –60.6 (*s*, CF₃). ESI-MS: 283 (100, $[\text{M} + \text{H}]^+$). HR-ESI-MS: 283.1177 ($[\text{M} + \text{H}]^+$, $\text{C}_{13}\text{H}_{10}\text{F}_3\text{N}_2\text{O}_2^+$; calc. 283.0689).

N-[3-Fluoro-4-(trifluoromethyl)[1,1'-biphenyl]-4-yl]urea (**6**). To a soln. of **4** (100 mg, 0.392 mmol, 1.0 equiv.) in CH_2Cl_2 (4.67 ml) was added ClSO_2NCO (52.8 μl , 0.608 mmol, 1.55 equiv.). The mixture was stirred at r.t. for 3 h, during which a white precipitate was formed. The reaction was then quenched with H_2O (4.67 ml), and the mixture was stirred at r.t. for 18 h. The mixture was filtered, washed with H_2O (20 ml), and dried *in vacuo*. Purification by FC (20–70% AcOEt/hexane) gave **6** (71.2 mg, 61%). White amorphous powder. R_f (50% AcOEt/hexane) 0.21. Anal. HPLC: 99.3% purity, t_R 7.43 min. M.p. 286–287°. $^1\text{H-NMR}$ ((D_6) DMSO): 8.50 (*d*, $J = 2.2$, NH); 8.29 (*t*, $J = 8.6$, 8.6, HNCCH); 7.86 (*d*, $J = 8.2$, $\text{F}_3\text{CC}(\text{CH})_2$); 7.77 (*d*, $J = 8.3$, $\text{F}_3\text{C}(\text{CH})_2(\text{CH})_2\text{CC}$); 7.64 (*dd*, $J = 2.1$, 12.9, FCCH); 7.51 (*dd*, $J = 1.8$, 8.6, HNCCHCHCC); 6.26 (*s*, NH₂). $^{13}\text{C-NMR}$ ((D_6) DMSO): 155.5 (C=O); 153.0 (CNH); 150.6 (CF); 142.7 (CCCHCF); 131.6 (CCF₃); 131.5 (FCCHCC); 126.9 ($\text{F}_3\text{CC}(\text{CH})_4\text{C}$); 125.7 (CF₃); 122.9 (CCCHCH); 120.3 (HNCCH); 113.1 (FCCH). $^{19}\text{F-NMR}$ ((D_6) DMSO): –60.9 (*s*, CF₃); –130.0 (*t*, $J = 10.9$, 11.4, arom. F). ESI-MS: 299 (100, $[\text{M} + \text{H}]^+$). HR-ESI-MS: 299.0799 ($[\text{M} + \text{H}]^+$, $\text{C}_{14}\text{H}_{11}\text{F}_4\text{N}_2\text{O}^+$; calc. 299.0802).

N-[3-Fluoro-4-(trifluoromethyl)[1,1'-biphenyl]-4-yl]thiourea (**7**). To a soln. of **4** (1.10 g, 4.33 mmol, 1.0 equiv.) in H_2O (8.66 ml) and 1M HCl (8.66 ml) was added NH_4SCN (822 mg, 10.8 mmol, 2.5 equiv.), and the mixture was heated at 140° for 5 h to give a white solid in a colorless soln. The mixture was then cooled to r.t. and poured onto ice (2.62 g), washed with cold H_2O (20 ml), and placed in an ice/water bath overnight. The white precipitate was collected by filtration and dried *in vacuo*. The residue was purified by FC (20–60% AcOEt/hexane) to give **7** (1.03 g, 76%). White amorphous powder. R_f (50% AcOEt/hexane) 0.32. Anal. HPLC: 99.8% purity, t_R 7.64 min. M.p. 186–187°. $^1\text{H-NMR}$ ((D_6) DMSO): 9.50 (*s*, NH); 7.94 (*m*, $\text{F}_3\text{CC}(\text{CH})_2(\text{CH})_2\text{CCCHCHCNH}$); 7.81 (*d*, $J = 8.4$, $\text{F}_3\text{C}(\text{CH})_2(\text{CH})_2\text{CC}$); 7.69 (*dd*, $J = 2.0$, 12.0, FCCH); 7.57 (*dd*, $J = 1.8$, 8.4, HNCCHCHCC). $^{13}\text{C-NMR}$ ((D_6) DMSO): 182.0 (C=S); 156.9 (CNH); 154.5 (CF); 142.4 (CCCHCF); 136.8 (CCF₃); 136.7 (FCCHCC); 127.7 (HNCCH); 127.3 ($\text{F}_3\text{CC}(\text{CH})_4\text{C}$); 125.8 (CF₃); 122.5 (CCCHCH); 114.2 (FCCH). $^{19}\text{F-NMR}$ ((D_6) DMSO): –61.0 (*s*, CF₃); –122.8 (*s*, arom. F). ESI-MS: 315 (100, $[\text{M} + \text{H}]^+$). HR-ESI-MS: 315.0556 ($[\text{M} + \text{H}]^+$, $\text{C}_{14}\text{H}_{11}\text{F}_4\text{N}_2\text{S}^+$; calc. 315.0574).

N-[3-Fluoro-4-(trifluoromethyl)[1,1'-biphenyl]-4-yl]sulfamide (**8**). To a soln. of ClSO_2NCO (37.2 μl , 0.427 mmol, 1.09 equiv.) in MeCN (0.91 ml) at 0° was added H_2O (7.69 μl , 0.427 mmol, 1.09 equiv.). The mixture was stirred at 0° for 1 min, then allowed to warm to r.t., and stirred for a further 3 h at the same temp. Then, the mixture was cooled to 0°, and a soln. of **4** (100 mg, 0.392 mmol, 1.0 equiv.) in pyridine (63.4 μl , 0.784 mmol, 2.0 equiv.) and MeCN (0.90 ml) was added dropwise over 2 min. The mixture was allowed to warm to r.t. and stirred for an additional 15 h. The pale-yellow soln. was subsequently diluted with H_2O (50 ml), washed with sat. aq. NaCl (10 ml), extracted with AcOEt (3 × 50 ml), dried (Na_2SO_4), and concentrated under reduced pressure. Purification by FC (10–30% AcOEt/hexane) gave **8** (69.4 mg, 53%). White amorphous powder. R_f (30% AcOEt/hexane) 0.33. Anal. HPLC: 98.9% purity, t_R 7.74 min. M.p. 151–152°. $^1\text{H-NMR}$ ((D_6) DMSO): 9.34 (*br. s*, NH); 7.92 (*d*, $J = 8.2$, $\text{F}_3\text{CC}(\text{CH})_2$); 7.80 (*d*, $J = 8.4$, $\text{F}_3\text{C}(\text{CH})_2(\text{CH})_2\text{CC}$); 7.66 (*dd*, $J = 1.9$, 12.1, FCCH); 7.58 (*m*, HNC(CH)₂CC); 7.23 (*s*, NH₂). $^{13}\text{C-NMR}$ ((D_6) DMSO): 155.2 (CNH); 152.8 (CF); 142.4 (CCCHCF); 134.8 (CCF₃); 134.7 (FCCHCC); 126.9 ($\text{F}_3\text{CC}(\text{CH})_4\text{C}$); 125.7 (CF₃); 123.4 (CCCHCH); 122.9 (HNCCH); 114.15 (FCCH). $^{19}\text{F-NMR}$ ((D_6) DMSO): –60.9 (*s*, CF₃); –124.4 (*dd*, $J = 7.2$, 12.2, arom. F). ESI-MS: 357 (100, $[\text{M} + \text{Na}]^+$). HR-ESI-MS: 357.0289 ($[\text{M} + \text{Na}]^+$, $\text{C}_{13}\text{H}_{10}\text{F}_4\text{N}_2\text{NaO}_2\text{S}^+$; calc. 357.0291). Data in accordance those in [14].

N-[3-Nitro-4-(trifluoromethyl)[1,1'-biphenyl]-4-yl]urea (**9**). To a soln. of **5** (100 mg, 0.355 mmol, 1.0 equiv.) in CH_2Cl_2 (4.20 ml), was added ClSO_2NCO (61.6 μl , 0.710 mmol, 2.0 equiv.) at 70°, and the mixture was heated at reflux the same temp. for 5 h during which a dark-red soln. was obtained. The reaction was then quenched with H_2O (4.20 ml) to give a white precipitate, and the mixture was stirred at r.t. for a further 48 h. The mixture was then filtered, washed with H_2O (20 ml) and sat. aq. NaHCO_3 , and

dried *in vacuo*. Purification by FC (1–15% MeOH/CH₂Cl₂) gave **9** (49.4 mg, 43%). White amorphous powder. *R_f* (70% AcOEt/hexane) 0.23. Anal. HPLC: 91.5% purity, *t_R* 8.86 min, eluted with isocratic 40% MeCN/H₂O with 0.1% TFA. M.p. 315–318°. ¹H-NMR ((D₆)DMSO): 8.24 (*d*, *J* = 2.2, NH); 7.99 (*s*, O₂NCC_H); 7.83 (*s*, F₃C(CH)₂(CH)₂CC); 7.80 (*s*, HNCCH); 6.18 (*s*, H₂N). ¹³C-NMR ((D₆)DMSO): 156.6 (C=O); 144.1 (CNH); 141.7 (CNO₂); 132.6 (CCCHCNO₂); 131.9 (CCF₃); 131.1 (NO₂CCHCC); 126.8 (F₃CC(CH)₄C); 125.7 (CF₃); 122.8 (HNCCH); 121.4 (HNCCHCH); 121.4 (O₂NCC_H). ¹⁹F-NMR ((D₆)DMSO): –60.9 (*s*, CF₃). ESI-MS: 326 (100, [M+H]⁺). HR-ESI-MS: 326.2238 ([M+H]⁺, C₁₄H₁₁F₃N₃O₃; calc. 326.2086).

N-[3-Nitro-4-(trifluoromethyl)[1,1'-biphenyl]-4-yl]thiourea (**10**). To a soln. of **5** (100 mg, 0.355 mmol, 1.0 equiv.) in H₂O (423 μl) and 1.0M HCl (355 μl) was added NH₄SCN (54.0 mg, 0.710 mmol, 2.0 equiv.), and the mixture was heated at 150° for 18 h. The mixture was subsequently cooled to r.t., poured onto ice (2.32 g), washed with cold H₂O (20 ml) and sat. aq. NaHCO₃, and placed in an ice-bath for 1 h. The brown precipitate formed was filtered on a pad of silica gel and dried *in vacuo*. The residue was purified by FC (60–90% AcOEt/hexane) to give **10** (25.0 mg, 21%). Brown amorphous powder. *R_f* (90% AcOEt/hexane) 0.83. Anal. HPLC: 98.2% purity, *t_R* 12.4 min, eluted with isocratic 50% MeCN/H₂O with 0.1% TFA. M.p. 306–308°. ¹H-NMR ((D₆)DMSO): 12.7 (*br. s*, NH₂); 7.91 (*d*, 7.1, F₃CC(CH)₂); 7.83 (*d*, *J* = 7.3, F₃C(CH)₂(CH)₂); 7.54 (*d*, *J* = 7.8, HNCCH); 7.45 (*s*, O₂NCC_H); 7.29 (*d*, 8.0, HNCCHCH). ¹³C-NMR ((D₆)DMSO): 169.1 (C=S); 144.2 (CNO₂); 142.4 (CNH); 133.1 (O₂NCC_H); 132.6 (CCF₃); 132.4 (O₂NCC_H); 127.4 (F₃CC(CH)₄C); 125.8 (CF₃); 121.8 (HNCCH); 109.9 (HNCCHCH); 107.7 (O₂NCC_H). ¹⁹F-NMR ((D₆)DMSO): –61.2 (*s*, CF₃). ESI-MS: 342 (100, [M+H]⁺). HR-ESI-MS: 342.9828 ([M+H]⁺, C₁₄H₁₁F₃N₃O₂S⁺; calc. 342.9711).

N-[3-Fluoro-4-(trifluoromethyl)[1,1'-biphenyl]-4-yl]benzamide (**12**). To a soln. of **4** (70.0 mg, 0.274 mmol, 1.0 equiv.) in Et₃N (37.9 μl) and CH₂Cl₂ (1.26 ml) was added PhCOCl (47.9 μl, 0.411 mmol, 1.5 equiv.), and the mixture was heated at 50° for 18 h. The mixture was subsequently cooled to r.t., washed with CH₂Cl₂ (50 ml) and sat. aq. NaHCO₃, and extracted with CH₂Cl₂ (3 × 30 ml). The combined org. layers were washed with brine and concentrated *in vacuo*. Purification by FC (0–40% AcOEt/hexane) gave **12** (107 mg, 99%). White amorphous powder. *R_f* (20% AcOEt/hexane) 0.37. Anal. HPLC: 98.6% purity, *t_R* 10.3 min, eluted with isocratic 70% MeCN/H₂O with 0.1% TFA. M.p. 210–211°. ¹H-NMR ((D₆)DMSO): 10.23 (*br. s*, NH); 8.01 (*d*, *J* = 7.2, C(O)C(CH)₂); 7.97 (*d*, *J* = 8.2, F₃CC(CH)₂); 7.83 (*d*, *J* = 8.3, F₃CC(CH)₂(CH)₂); 7.80 (*d*, *J* = 8.4, HNCCH); 7.75 (*m*, FCCH); 7.65 (*s*, HNCCHCH); 7.62 (*d*, *J* = 7.4, C(O)C(CH)₂(CH)₂CH); 7.55 (*t*, *J* = 7.6, 7.4, C(O)C(CH)₂(CH)₂). ¹³C-NMR ((D₆)DMSO): 165.5 (C=O); 157.0 (CF); 154.5 (HNC); 142.4 (FCCHCC); 137.0 (FCCHCC); 136.9 (F₃CC); 133.8 (C(O)C); 131.9 (C(O)C(CH)₂(CH)₂CH); 128.4 (C(O)C(CH)₂(CH)₂CH); 127.8 (C(O)C(CH)₂(CH)₂CH); 127.4 (F₃CC(CH)₂(CH)₂); 127.1 (HNCCH); 125.8 (CF₃); 122.8 (HNCCHCH); 114.3 (FCC). ¹⁹F-NMR ((D₆)DMSO): –61.4 (*s*, CF₃). ESI-MS: 360 (100, [M+H]⁺). HR-ESI-MS: 360.1010 ([M+H]⁺, C₂₀H₁₄F₄NO⁺; calc. 360.1006).

N-[3-Fluoro-4-(trifluoromethyl)[1,1'-biphenyl]-4-yl]-3-methylbutanamide (**13**). To a soln. of **4** (70.0 mg, 0.274 mmol, 1.0 equiv.) in Et₃N (37.9 μl) and CH₂Cl₂ (1.26 ml) was added 3-methylbutanoyl chloride (50.6 μl, 0.411 mmol, 1.5 equiv.), and the mixture was stirred at r.t. for 24 h. The mixture was subsequently cooled to r.t. and washed with CH₂Cl₂ (50 ml) and sat. aq. NaHCO₃, and extracted with CH₂Cl₂ (3 × 30 ml). The combined org. layers were washed with brine (30 ml) and concentrated *in vacuo*. Purification by FC (0–40% AcOEt/hexane) gave **13** (90.1 mg, 88%). White amorphous powder. *R_f* (20% AcOEt/hexane) 0.38. Anal. HPLC: 98.5% purity, *t_R* 10.4, eluted with isocratic 70% MeCN/H₂O with 0.1% TFA. M.p. 159–160°. ¹H-NMR ((D₆)DMSO): 9.76 (*br. s*, NH); 8.03 (*t*, *J* = 8.3, 8.4, HNCCH); 7.92 (*d*, *J* = 8.2, F₃CC(CH)₂); 7.80 (*d*, *J* = 8.3, F₃CC(CH)₂(CH)₂); 7.69 (*dd*, *J* = 12.2, 1.7, FCCH); 7.57 (*dd*, *J* = 8.4, 1.3, HNCCHCH); 2.29 (*d*, *J* = 7.2, C(O)C(CH)₂); 2.09 (*dt*, *J* = 13.6, 6.8, C(O)C(CH)₂CH); 0.95 (*d*, *J* = 6.6, Me₂CH). ¹³C-NMR ((D₆)DMSO): 171.2 (C=O); 155.0 (CF); 152.6 (HNC); 142.4 (FCCHCC); 135.2 (FCCHCC); 127.2 (F₃CC(CH)₂(CH)₂); 126.5 (F₃CC); 125.8 (CF₃); 124.4 (HNCCH); 122.7 (HNCCHCH); 44.9 (C(O)C); 25.6 (C(O)CH₂C); 22.2 (Me₂CH). ¹⁹F-NMR ((D₆)DMSO): –60.8 (*s*, CF₃). ESI-MS: 340 (100, [M+H]⁺). HR-ESI-MS: 340.1323 ([M+H]⁺, C₁₈H₁₈F₄NO; calc. 340.1319).

Density-Functional Theory (DFT) Calculations. Calculations were conducted using DFT [21][22] as implemented in the Gaussian09, suite of *ab initio* quantum chemistry programs [18]. Geometry optimizations and vibrational frequency calculations were performed with a restricted scheme using the

hybrid-DFT B3LYP exchange-correlation functionals and the all electron double- ζ 6-31 + + G(d,p) basis set by Pople and co-workers for all atoms. Normal SCF and geometry convergence criteria were used throughout, and no symmetry constraints were imposed. Harmonic frequency analysis based on analytical second derivatives was used to characterize the optimized geometries as local minima.

Cloning, Expression, and Purification of the Human KSP (Kif11/Eg5) Motor Domain. A synthetic cDNA fragment encoding residues 1–368 of human Kif11 and codon-optimized for bacterial expression was cloned into pSTCm1, a modified pET47b vector. The plasmid was transformed to chemically competent BL21[DE3] bacterial cells, plated onto LB-Kan plates, and incubated overnight at 37°. A single colony was picked and used to inoculate a 100-ml LB-Kan overnight culture which was grown at 37° in an incubator shaker (200 rpm). 4L of LB-Kan were inoculated with 20 ml (1:50) of the overnight culture and grown in an incubator shaker at 37° and 200 rpm to an OD of 0.6. The temp. was lowered to 20° before induction with 1 mM IPTG, and incubation was continued overnight at 20° and 200 rpm.

Cells were harvested by centrifugation, and the pellet was taken up in 50 ml of lysis buffer, 50 mM Tris (pH7.5), 500 mM NaCl, 10 mM 1H-imidazole, 10 mM β -mercaptoethanol, 1 protease inhibitor cocktail tablet (Complete EDTA free; Roche Diagnostics). Cells were lysed on ice by using a Vibra Cell sonication device (Sonics) equipped with a large prep. sonication tip by applying three 1-min sonication bursts at 100% amplitude. The lysate was cleared by 25000g centrifugation step (1 h) and passed through a 0.45- μ m filtration step.

The protein was subsequently purified using IMAC, followed by a size-exclusion chromatography on an ÄKTA Xpress chromatography machine. The filtered supernatant was applied on a 5-ml HisTrap crude FF column and washed with 20CV (column volumes) of wash buffer 1 (50 mM Tris (pH7.5), 500 mM NaCl, 10 mM 1H-imidazole, 10 mM β -mercaptoethanol) and 20CV wash buffer 2 (50 mM Tris (pH7.5), 500 mM NaCl, 60 mM 1H-imidazole, 10 mM β -mercaptoethanol). The protein was eluted using 5CV of elution buffer (50 mM Tris (pH7.5), 500 mM NaCl, 500 mM 1H-imidazole, 10 mM β -mercaptoethanol). The eluted protein was loaded onto a 16/60 HiLoad Superdex200 size-exclusion column equilibrated with 20 mM Tris·HCl (pH7.5) and 150 mM NaCl. The total yield was ca. 15 mg of pure protein.

Kinesin Motor Protein ATP-Hydrolase Inhibition Assay. Inhibition of the ATP-hydrolase activity of various kinesin motor proteins was measured by using the Kinesin ATPase End-Point Biochem Kit, BK053 (Cytoskeleton, Denver, USA). Generation of inorg. phosphate (P_i) during MT-activated ATP-hydrolase activity of kinesin motor proteins was measured at 650 nm. The concentration of the motor proteins (2.5 μ g of total protein) used in the assay was kept as low as possible to minimize possible crowding effects on MTs. Compounds were diluted to give final concentrations of 1.0 μ M and were incubated at r.t. for 10–20 min. Assays were conducted in accordance with the manufacturer's protocol.

Antiproliferative MTT Assays (in vitro). DU-145, PC-3, MCF-7, and SKOV3 cell lines, cell culture media, and additives were obtained from BioConcept (CH-Allschwil). Cells were grown in plastic tissue culture flasks. For PC-3 cells, Dulbecco's Modified Eagle's Medium (DMEM) with 10% Fetal Calf Serum (FCS; v/v) was supplemented with glutamine (2 mM) and antibiotics (penicillin (100 units/ml), streptomycin (100 μ g/ml), and fungizone (0.25 μ g/ml)). For DU-145 cells, Minimum Essential Medium Eagle (MEM) with 10% FCS (v/v), glutamine (2 mM), and antibiotics was supplemented with sodium pyruvate (1 mM), sodium bicarbonate (1.5 g/l), and 1% non-essential amino acids (NEAA). For MCF-7 cells, DMEM with Nutrient Mixture F-12 Ham (Ham's F-12) and 10% FCS (v/v) was supplemented with glutamine (2 mM) and antibiotics (penicillin (100 units/ml), streptomycin (100 μ g/ml), and fungizone (0.25 μ g/ml)). For SKOV-3 cells, DMEM with 10% FCS and glutamine (2 mM) was supplemented with antibiotics (penicillin (100 units/ml), streptomycin (100 μ g/ml), and fungizone (0.25 μ g/ml)). All the cells were maintained at 37° with 5% CO₂.

Test compounds, in DMSO stock solns., were prepared in concentrations ranging from 1.0 nM to 1.0 mM. The test compounds were serially diluted (1:4) with growth medium and then diluted into the cell assay plate with a final DMSO concentration of \leq 0.2%. Cells were plated in duplicate 96-well plates with a density of 2000 cells/well with the exception of MCF-7, where cell density was 1000 cells/well, and allowed to adhere for 24 h. Cells were then exposed to the test compounds which were added directly to the media. Appropriate controls for culture media and vehicle were used throughout to measure non-specific background, and to serve as a reference to each cell line. Plates were incubated at 37° for 44 h.

then treated with MTT soln., and cultured for 2–4 h. After removing the media, DMSO (100 μ l/well) was added to solubilize the purple formazan product. Electronic absorbance was then measured at 560 nm with *Perkin-Elmer Victor™ X3 Multilabel Plate Reader*. The extent of growth inhibition was determined by nonlinear regression analysis of a plot of absorbance (560 nm) vs. drug concentration (μ M), and analyzed with GraphPad Prism 5. Data are reported as the average of four quadruplet runs, and the statistical limits for the data are reported to be within the 95% confidence interval.

Flow Cytometry. DU-145, PC-3, MCF-7, and SKOV3 cell lines were grown in DMEM supplemented with 10% fetal bovine serum and 1 unit/ml penicillin-streptomycin. Cells were plated onto 100 mm² dishes at a cell density of 1.0×10^6 cells/dish, and 24 h later, they were treated with 1.0 μ M of the biphenyl compound. Cells were harvested 24 h after treatment. The culture medium was collected, and the floating cells were collected by short centrifugation (5 min at 1000 rpm). Attached cells were washed once with ice-cold PBS (5 ml), detached by treatment with trypsin/EDTA soln. (3 ml) at 37° for ca. 5 min, and, together with the detached floating cells, were transferred into 15 ml *Falcon* tubes. The cell culture dish was washed with DMEM (10 ml) to collect all the remaining cells. After centrifugation for 5 min at 1000 rpm at r.t., the supernatant was discarded, and the cell pellet was washed twice with 10 ml PBS. The supernatant was discarded, and the cells were resuspended in 4 ml of ice-cold fixation soln. (70 vol% EtOH, 30 vol% H₂O) and stored at –20° for 24 h. Thereafter, PBS (10 ml) stored at 4° was added to the cells before centrifugation for 5 min at 1000 rpm. The supernatant was discarded, and the cell pellet was washed once with PBS (10 ml; 4°). The cell pellet was resuspended in 1.0 ml of staining soln. containing 0.1 mg/ml RNase A (*Sigma-Aldrich*), 50 μ g/ml propidium iodide (PI) from 2.5 mg/ml stock soln., and 0.05% *Triton X-100* (*Fluka*) in PBS. After incubation at 37° for 40 min in the dark, PBS (3 ml) was added, and the cell pellet was collected by centrifugation for 5 min at 1500 rpm, followed by the removal of the supernatant. The pellet was suspended in PBS (500 μ l) and analyzed using the *Millipore easyCyte HT* flow cytometry system (excitation, 488 nm, emission, 583 nm). Data were analyzed by cell-cycle analysis software (*Flowjo, TreeStar Inc.*).

Western Blot. DU-145, PC-3, MCF-7, and SKOV-3 cells were grown in 10-cm dishes to ca. 70% confluence in DMEM containing 10% FCS and incubated at 37° for 24 h. Cells were then treated with 1.0 μ M of biphenyl compounds and incubated at 37° for 24 h. Cells were washed twice with PBS and lysed on ice in a lysis buffer consisting of 0.1M NaCl, 0.05M *Tris*·His (pH 7.5), 1% *Triton X-100*, 0.001M ethylenediaminetetraacetic acid (EDTA), 0.01M β -glycerophosphate, 0.02M sodium vanadate, and protease inhibitor cocktail *Complete™* (*Roche Diagnostics, Switzerland*).

Lysates were cleared by centrifugation, and 20 μ g of protein, as determined by the 'Advanced Protein Assay' (*Sigma-Aldrich, CH-Buchs*), were separated by SDS-PAGE (7.5%) under reducing conditions and transferred to a polyvinylidene fluoride (PVDF) membrane (*Millipore AG, CH-Zug*) with a semi-dry blotting device (*BioRad Laboratories AG, CH-Reinach*). Incubations with primary antibodies (Cyclin B1, Cyclin E, and Phospho-Histone H3) were performed according to the manufacturer's protocol at 4° overnight in TBST (0.14M NaCl, 0.02M *Tris*·1.1 HCl (pH 7.5), 0.1% *Tween 20*) containing 2% bovine serum albumin (BSA). Detection was accomplished with secondary HRP-linked antibodies (3 μ l in 15 ml for 30 min) from *Cell Signalling Technology®* (*Bioconcept*) and the *ECL* chemiluminescence kit from *Pierce (Perbio Science Switzerland SA, CH-Lausanne)*.

Confocal Fluorescence Microscopy. *Permeabilization Buffer* (prepared fresh). A 10 \times permeabilization buffer was prepared as a stock soln. (1.54M NaCl, 15.44 mM KH₂PO₄, 28.58 mM Na₂HPO₄·7 H₂O, and 5% *Triton X-100*). To 10 \times permeabilization buffer (5 ml) were added 40 ml deionized H₂O. The pH was adjusted to pH7.2, and then the soln. was diluted to 50 ml to make a 1.0 \times permeabilization buffer stock soln. Stock solns. can be kept for several weeks in a refrigerator. To 1.0 \times permeabilization buffer (2.4 ml) were added 9.6 ml PBS to give 0.2 \times permeabilization buffer used as working soln.

Blocking Buffer. A soln. of PBS containing 1% BSA and 0.3% *Tween-20* was prepared.

Confocal Fluorescence Microscopy. Cells lines, cell culture media, and additives were obtained from *BioConcept*. Cells were maintained at 37° with 5% CO₂ and were placed in 8-well *Lab-Tek II Chamber Slides* (*NUNC, VWR, LabShop, Batavia, IL*) with a density of 5000 cells/well, and allowed to adhere for 24 h and to grow to 80% confluence. Cells were then exposed to 1.0 μ M concentrations of biphenyl compounds and incubated for 22 h at 37°. All plates contained wells with culture media only to serve as a reference control to the SKOV-3 cell line.

Cells were washed with PBS ($3 \times 400 \mu\text{l}$), incubated with freshly prepared, pre-warmed 4% paraformaldehyde ($400 \mu\text{l}$) for 15 min at 37° , washed with PBS ($3 \times 400 \mu\text{l}$), incubated with a freshly made $0.2 \times$ permeabilization buffer ($300 \mu\text{l}$) for 15 min at 37° , washed with PBS ($3 \times 400 \mu\text{l}$), incubated with 1 drop of *ImageItFX* (Invitrogen ‘Signal Enhancer’) for 30 min, washed with PBS ($3 \times 400 \mu\text{l}$) and incubated with primary antibody ($250 \mu\text{l}$, Mouse α -tubulin (1:1000 dilution in blocking buffer; *Sigma-Aldrich*)) at 37° for 2 h. Then, cells were washed with PBS ($3 \times 400 \mu\text{l}$), incubated with secondary antibody ($250 \mu\text{l}$, Goat a-Mouse *Alexa 568* α -tubulin staining (Invitrogen), 1:2000 dilution in blocking buffer) at 37° for 1.5 h then washed with PBS ($3 \times 400 \mu\text{l}$), incubated with *Hoechst 33342* 1:100000 in deionized H_2O for 10 min, and finally washed with deionized H_2O ($3 \times 400 \mu\text{l}$). Slides were drained, and all areas surrounding the tissue were dried, mounted onto microscope slides with one drop of *Prolong Gold* (Invitrogen), sealed with nail polish (*Gemey, Express Finish*), and kept in the dark at 4° .

Images were captured using a *Zeiss LSM 510* laser-scanning confocal microscope, $63 \times$ oil *DIC Plan-Apochromat* objective, 1.4NA. The microscope was incubated in an *EMBL* incubator box *GP 168* at 36.5° . Solid-state (561–10 nm) and dDiode (405–430 nm) laser lines were used to image *Alexa 568* α -tubulin staining and *Hoechst 33342*, resp. Images were processed using AIM LSM4.0 software (*Carl Zeiss*) and ImageJ (National Institutes of Health, USA).

REFERENCES

- [1] D. Hanahan, R. A. Weinberg, *Cell* **2011**, *144*, 646.
- [2] M. Schmidt, H. Bastians, *Drug Resistance Updates* **2007**, *10*, 162.
- [3] C. Dumontet, M. A. Jordan, *Nat. Rev. Drug Discovery* **2010**, *9*, 790.
- [4] T. U. Mayer, T. M. Kapoor, S. J. Haggarty, R. W. King, S. L. Schreiber, T. J. Mitchison, *Science* **1999**, *286*, 971.
- [5] V. Sarli, A. Giannis, *Clin. Cancer Res.* **2008**, *14*, 7583.
- [6] N. Hirokawa, Y. Noda, *Physiol. Rev.* **2008**, *88*, 1089.
- [7] R. Sakowicz, M. S. Berdelis, K. Ray, C. L. Blackburn, C. Hopmann, D. J. Faulkner, L. S. B. Goldstein, *Science* **1998**, *280*, 292.
- [8] R. Sakowicz, J. T. Finer, C. Beraud, A. Crompton, E. Lewis, A. Fritsch, Y. Lee, J. Mak, R. Moody, R. Turincio, J. C. Chabala, P. Gonzales, S. Roth, S. Weitman, K. W. Wood, *Cancer Res.* **2004**, *64*, 3276.
- [9] B. Zhang, J.-F. Liu, Y. Xu, S.-C. Ng, *Biochem. Biophys. Res. Commun.* **2008**, *372*, 565.
- [10] A. I. Marcus, U. Peters, S. L. Thomas, S. Garrett, A. Zelnak, T. M. Kapoor, P. Giannakakou, *J. Biol. Chem.* **2005**, *280*, 11569.
- [11] J. W. Purcell, J. Davis, M. Reddy, S. Martin, K. Samayoa, H. Vo, K. Thomsen, P. Bean, W. L. Kuo, S. Ziyad, J. Billig, H. S. Feiler, J. W. Gray, K. W. Wood, S. Cases, *Clin. Cancer Res.* **2010**, *16*, 566.
- [12] K. Kim, Y. Xie, E. Tytler, R. Woessner, G. Mor, A. Alvero, *J. Translat. Med.* **2009**, *7*, 63.
- [13] L. Luo, C. A. Parrish, N. Nevins, D. E. McNulty, A. M. Chaudhari, J. D. Carson, V. Sudakin, A. N. Shaw, R. Lehr, H. Zhao, S. Sweitzer, L. Lad, K. W. Wood, R. Sakowicz, R. S. Annan, P. S. Huang, J. R. Jackson, D. Dhanak, R. A. Copeland, K. R. Auger, *Nat. Chem. Biol.* **2007**, *3*, 722.
- [14] C. A. Parrish, N. D. Adams, K. R. Auger, J. L. Burgess, J. D. Carson, A. M. Chaudhari, R. A. Copeland, M. A. Diamond, C. A. Donatelli, K. J. Duffy, L. F. Faucette, J. T. Finer, W. F. Huffman, E. D. Hugger, J. R. Jackson, S. D. Knight, L. Luo, M. L. Moore, K. A. Newlander, L. H. Ridgers, R. Sakowicz, A. N. Shaw, C.-M. M. Sung, D. Sutton, K. W. Wood, S.-Y. Zhang, M. N. Zimmerman, D. Dhanak, *J. Med. Chem.* **2007**, *50*, 4939.
- [15] K. Matsuno, J.-i. Sawada, M. Sugimoto, N. Ogo, A. Asai, *Bioorg. Med. Chem. Lett.* **2009**, *19*, 1058.
- [16] M. Wang, M. Gao, B. H. Mock, K. D. Miller, G. W. Sledge, G. D. Hutchins, Q.-H. Zheng, *Bioorg. Med. Chem.* **2006**, *14*, 8599.
- [17] N. Miyaura, A. Suzuki, *Chem. Rev.* **1995**, *95*, 2457.
- [18] M. J. Frisch, G. W. Trucks, H. B. Schlegel, G. E. Scuseria, M. A. Robb, J. R. Cheeseman, J. A. Montgomery Jr., T. Vreven, K. N. Kudin, J. C. Burant, J. M. Millam, S. S. Iyengar, J. Tomasi, V. Barone, B. Mennucci, M. Cossi, G. Scalmani, N. Rega, G. A. Petersson, H. Nakatsuji, M. Hada, M. Ehara, K. Toyota, R. Fukuda, J. Hasegawa, M. Ishida, T. Nakajima, Y. Honda, O. Kitao, H. Nakai,

- M. Klene, X. Li, J. E. Knox, H. P. Hratchian, J. B. Cross, V. Bakken, C. Adamo, J. Jaramillo, R. Gomperts, R. E. Stratmann, O. Yazyev, A. J. Austin, R. Cammi, C. Pomelli, J. W. Ochterski, P. Y. Ayala, K. Morokuma, G. A. Voth, P. Salvador, J. J. Dannenberg, V. G. Zakrzewski, S. Dapprich, A. D. Daniels, M. C. Strain, O. Farkas, D. K. Malick, A. D. Rabuck, K. Raghavachari, J. B. Foresman, J. V. Ortiz, Q. Cui, A. G. Baboul, S. Clifford, J. Cioslowski, B. B. Stefanov, G. Liu, A. Liashenko, P. Piskorz, I. Komaromi, R. L. Martin, D. J. Fox, T. Keith, M. A. Al-Laham, C. Y. Peng, A. Nanayakkara, M. Challacombe, P. M. W. Gill, B. Johnson, W. Chen, M. W. Wong, C. Gonzalez, J. A. Pople, Gaussian 03, *Gaussian, Inc.*, Wallingford, CT, 2004.
- [19] F. H. Allen, O. Kennard, D. G. Watson, L. Brammer, A. G. Orpen, R. Taylor, *J. Chem. Soc., Perkin Trans. 2* **1987**, S1.
- [20] W. C. Still, M. Kahn, A. Mitra, *J. Org. Chem.* **1978**, *43*, 2923.
- [21] P. Hohenberg, W. Kohn, *Phys. Rev. B: Condens. Matter Mater. Phys.* **1964**, *136*, 864.
- [22] W. Kohn, L. J. Sham, University of California, La Jolla, CA, 1965, p. 21.

Received November 25, 2012